

DEPENDENCE OF DIPOLE LAYER ON GRAPHITE SURFACE ON SIZE OF CONTACTING GOLD NANOPARTICLES

S. W. Mugo

Department of Physics, Jomo Kenyatta University of Agriculture and Technology

E-mail: wawerumugo@jkuat.ac.uk

Abstract

The interfacial dipole on pyrolytic graphite surface shows a high dependence with size and coverage of gold nanoparticles. Small nanoparticles with an average size of 2.4 nm exhibit a large dipole moment, decreasing with increasing particle diameter. The value becomes negative for nanoparticles > 6 nm. The behaviour is described by charge densities created after charge transfer between individual gold nanoparticles and graphite surface. The subsequent decrease in dipole for large nanoparticles is shown to be due to depolarization effects. The study provides a novel method to control electronic properties at metal-graphite interface which is useful in graphene electronic devices and catalysis on support.

Key words: Graphene, charge transfer, SKPM, TEM, STEM, HRSTEM

1.0 Introduction

The development of ultrathin devices has deepened the need to understand materials' surface and interface electronic structures (Rusu *et al.*, 2010; Datta *et al.*, 2008). This is because as devices shrink in size, their properties are controlled by surface atoms causing a significant deviation from corresponding bulk material (Ohgi and Fujita, 2003; Blanter and Martin, 2007). Graphene/graphite nanostructures with metal contacts have emerged as a viable candidate in this application (Datta *et al.*, 2008; Blanter and Martin, 2007; Klusek *et al.*, 2009; Uchoa *et al.*, 2008; Sutter *et al.*, 2008; Benayad *et al.*, 2009). The unique behaviour arises from effects of charge transfer between graphite and contacting metal (Hayashi *et al.*, 2002; Lu *et al.*, 2006; Klusek *et al.*, 2009; Benayad *et al.*, 2009; Liu *et al.*, 2011; Giovannetti *et al.*, 2008). Experimentally, the charge transfer has been shown to depend on work function of contacting metal (Uchoa *et al.*, 2008; Giovannetti *et al.*, 2008; Huard *et al.*, 2008).

Recent studies based on density function theory (DFT) have shown additional dipole due to the bonding interactions involved (Huard *et al.*, 2008; Hamada and Otani, 2010; Gong *et al.*, 2010). For chemisorption, the strong interaction results in formation of metal carbide bonds, causing graphene/graphite π -orbital and metals d -orbital to hybridize (Liu *et al.*, 2011; Giovannetti *et al.*, 2008; Huard *et al.*, 2008; Gong *et al.*, 2010). In weak physisorption interaction, the overlap of electron wave function from metal causes a shift in graphite Fermi level (Uchoa *et al.*, 2008;

Giovannetti *et al.*, 2008; Gong *et al.*, 2010). The changing electronic structure produces an additional dipole making crossover in direction of charge transfer from either metal to graphite or vice versa shifted by 0.9 eV (Rusu *et al.*, 2010; Giovannetti *et al.*, 2008; Gong *et al.*, 2010; Jin *et al.*, 2010). This behaviour has so far been reported for uniform layer coverage and closest packing of metal atoms on graphite surface. However, deposited ultrathin metal films have different surface atom densities which may lead to different electronic structures and chemical reactivities (Ohgi and Fujita, 2003; Sun *et al.*, 2010; Gefen *et al.*, 1986; Young *et al.*, 2008; Wang *et al.*, 2006).

Our results reveal that the electronic dipole on graphite surface depends on size and coverage of contacting gold nanoparticles. Dipole is highest for small nanoparticles with an average size of 2.4 nm and decreases linearly with nanoparticle diameter. This is attributed to charge transfer between nanoparticles and graphite surface. The subsequent decrease in dipole and negative values measured for large nanoparticles > 6 nm is due to depolarization effects. The result demonstrates that synthesis of controlled metal particle sizes and densities on graphite can be an effective method to modify electronic properties which would otherwise be difficult to achieve with different metals of different work functions.

2.0 Materials and Methods

Graphitic nanostructures from synthetic highly ordered pyrolytic graphite (HOPG) were exfoliated through repeated peeling. Ultrathin gold films were then deposited through thermal deposition at 10^{-11} mbar. To influence the growth of films, graphite was cooled during deposition to -180 °C and the samples post annealed in H_2/Ar at 300 °C for 20 minutes. Surface potential measurements were immediately obtained in high vacuum with a JSPM 5200 atomic force microscope (AFM) equipped with a Kelvin controller. Reproducibility in the measured values was maintained by scanning the same position twice and on two other different regions of the sample. The process was then repeated on two other samples prepared in similar conditions. The final value was obtained from mean distributions. The data was also processed through two other methods: (i) averaging line profiles extending across full scan range and (ii) converting scans into binary images and masking out high contrast regions. Further analysis of the samples was conducted with transmission electron microscope (TEM) for morphology analysis and with a double aberration corrected scanning transmission electron microscope (STEM) in high angle annular dark field imaging mode (HAADF) to examine film nanostructure.

3.0 Results

3.1 Effect of Deposited Au Nominal Thickness on Graphite Surface Potential

Figure 1 displays surface potentials on graphite: (i) cooled to -180 °C, (ii) at room temperature, (iii) post-annealed cooled substrate (300 °C), and (iv) post-annealed

sample deposited at room temperature (300 °C). Measured surface potentials with Au nominal thickness (extracted from histogram distributions), shows linear increases. Each data consists of at least 8 measurements and with variations indicated by error bars. Values on “as deposited” films are larger than those obtained on bulk Au film and on fresh graphite surface. Changes are highest on Au deposited on cooled graphite. The values reduced drastically on annealed samples with films deposited at room temperature recording an even smaller value than was measured on either bulk Au or fresh graphite surface.

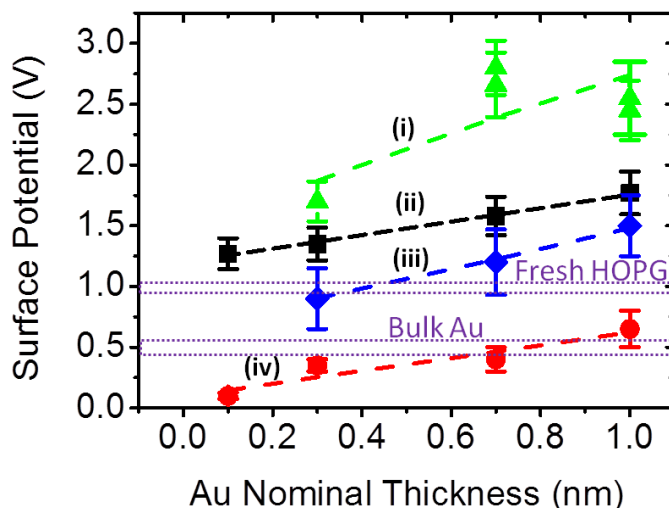


Fig. 1. Dependence of surface potential on growth conditions of Au deposited on graphite

By comparing data extracted from the three processing methods (histogram distribution, line profiles and masked high contrast regions), it was observed that the trends were similar. Variation was least on masked high contrast regions due to background uniformity.

3.2 Morphology of Ultrathin Au Films

TEM analysis revealed the ultrathin Au films to be discontinuous, consisting of discrete nanoparticles (Fig. 2 a). Most of these nanoparticles had a hexagonal shape (Fig. 2 b). Selected area electron diffraction (SAED) from single particles revealed an fcc structure consisting of spots superimposed on the ring, (Fig. 2c). Cooling the substrate significantly reduced significantly particle coalescence making the nanoparticles to be much smaller and increased concentration. Additionally, a large number of singular atoms from High Resolution STEM (HRSTEM) could be observed streaking on cooled graphite surface.

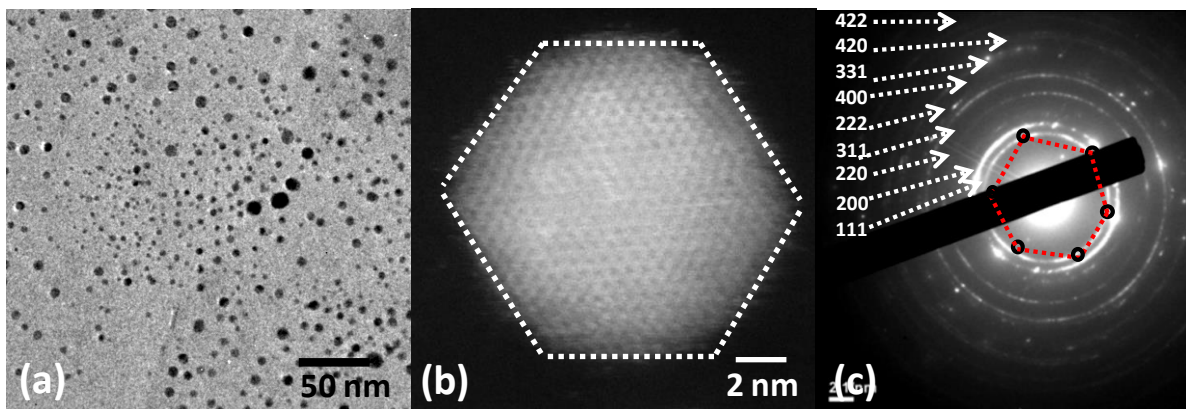


Fig. 2. 1 nm Au (a) STEM shows discrete particles (b) HRSTEM of single particle (c) SAED.

3.3 Change of Film Morphology with Annealing

After annealing, particle coalescence and agglomeration became dominant increasing the average particle sizes, Fig. 3a. For example for 1 nm deposited at room temperature, dramatic sintering of particles from an average diameter of 4.1 nm to 12.3 nm is observed. Average particle separation also increased from 2 nm to 10 nm. In contrast, nanoparticles on cooled substrates had reduced coalescence with average diameter increasing from 4 nm to 6 nm (Fig. 2a). Small particles retained the hexagonal shape but large particles did not conform to any geometry. The large particles had facets and stacking faults, Fig. 3b, which led to polycrystalline structure as revealed by SAED, Fig 3c. The diffuse reflection rings can be attributed to differently oriented lattices from the coalescing Au nanoparticles.

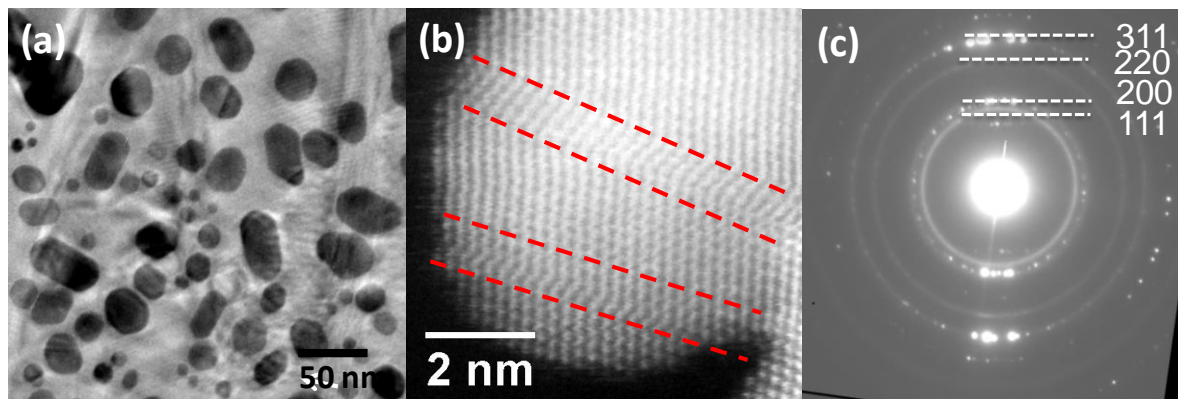


Fig. 3. 1 nm Au (a) particle coalescence after annealing due to (b) HRSTEM shows stacking faults, (c) SAED shows differently oriented lattices

Particle sizes were determined by approximating spherical geometry and measuring across their diameter. Analysis of more than 500 particles for each condition revealed that nanoparticles on cooled graphite were much smaller compared to those deposited at room temperature. The density of Au nanoparticles was

observed to increase linearly with nominal thickness, Fig. 4. On annealing, the linearity of nanoparticle density with nominal thickness was retained although values were much smaller due to the effects of coalescence.

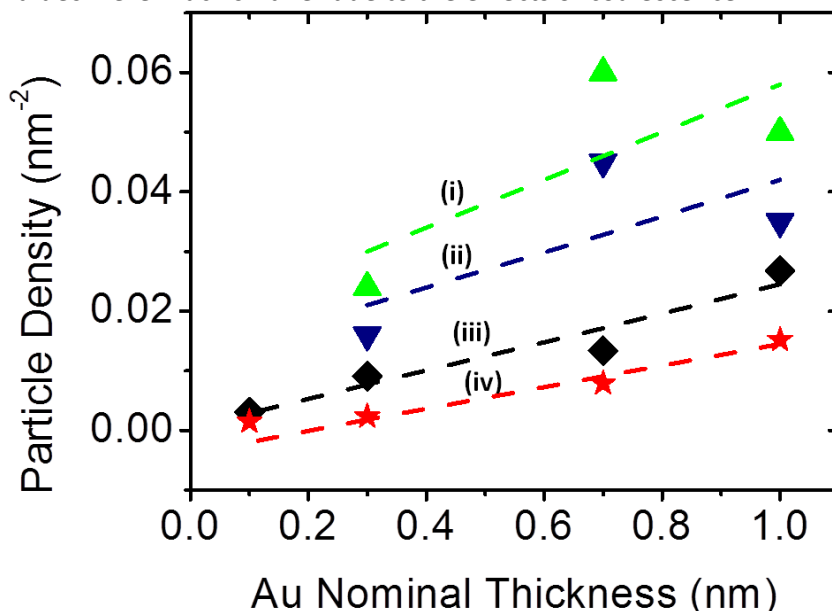


Fig. 4. Nanoparticle density increased linearly with Au nominal thickness for (i) cooled graphite (ii) post-annealed cooled graphite (iii) room temperature deposition (iv) post-annealed room temperature deposition.

4.0 Discussion

4.1 Growth of Au Nanoparticles on Graphite

Change in Au morphology (Fig. 2 and 3) can be understood from growth dynamics of thin films (Norrman *et al.*, 1978; Netterfield and Martin, 1986; Tang, 2003; Corain and Toshima, 2008). At room temperature, Au atoms arriving on graphite have increased kinetics moving around to nucleate with other atoms compared to cooled deposition. The high number of singular Au atoms on cooled deposition suggests strong interaction with graphite support.

The hexagonal geometry seen on small particles indicate that Au atoms are initially adsorbed in the hollow sites of graphite structure, consistent with the tendency of any system to minimize energy. Seeding crystals therefore develop in hexagonal arrangement mimicking graphite structure. Small nanoparticles have lower average surface energy making them have a lower probability of becoming mobile and combining (Somorjai, 1981; Corain and Toshima, 2008; Veith *et al.*, 2009). Thus, they are able to maintain their shape and structure. Polycrystalline structure from SAED indicates nanoparticles to consist of several sub-crystals. As more atoms are adsorbed, several nucleation points are established increasing particle density. The

0.26 nm lattice spacing measured on single atoms is close to elemental (111) d-spacing of bulk Au of 0.235 nm.

On annealing, the dramatic changes in particle shapes and sizes are due to coalescence and sintering. The flattened appearance on top surface of most nanoparticles (Fig. 3 b) is in contrast with Wulff construction which predicts particles to be rounded (Marks, 1994). This is due to particles of different orientation joining together (Barnard and Chen, 2011; Gai and Harmer, 2002). The high strain energy along the lattice mismatch regions resulted in formation of grain boundaries. Overlying atoms diffuse along the crystallite edges leading to reduction of atomic planes on the top surface. This is consistent with SAED from large particles where extra reflections were observed attributed to different orientations of crystal planes and presence of defects.

4.2 Influence of Nanoparticles Size to the Interfacial Dipole

The positive change in surface potential indicates electrons are transferred from graphite to Au, as governed by the polarity of Kelvin probe (Kelvin and Lassabater, 1898; Kikukawa *et al.*, 1995; Jacobs *et al.*, 1997; Rosenwaks *et al.*, 2004; Zerweck *et al.*, 2005; Palermo *et al.*, 2006). As the work function of gold is larger, electrons would flow from graphite (with a lower work function) to Au leaving excess holes on graphite and excess electrons on Au. This is also consistent with DFT theory that electron transfer from graphite to metal occurs when work function of metal is ≤ 5.4 eV (Liu *et al.*, 2011; Giovannetti *et al.*, 2008; Jin *et al.*, 2010). The charge transfer occurs from individual nanoparticles with graphite resulting in creation of surface dipoles. Neglecting contribution of bonding interaction between Au and graphite, since they are small compared with recorded changes, the dipoles from the nanoparticles sum to produce an average local dipole P , as graphite is conducting in c-axis. By definition, work function is the energy difference between electrostatic potential in vacuum and Fermi energy. Any change in electrostatic potential caused by these dipoles contributes to a net change in work function ΔW as governed by:

$$\Delta W = \left(\frac{N}{A} \right) \left(\frac{P_0 \cdot n}{\epsilon_0} \right) \quad (1)$$

where $N/A = \Delta n$ is the nanoparticles density, P_0 is dipole moment per unit area, n is unit direction normal to field and ϵ is permittivity of free space.

Figure 5 displays the calculated dipole as a function of nanoparticle diameters using equation 1. The large value on small particles is attributed to large surface area which increases the surface atom densities available for interaction with graphite. An increase in surface atoms results in high charge densities and which then depends on density of nanoparticles.

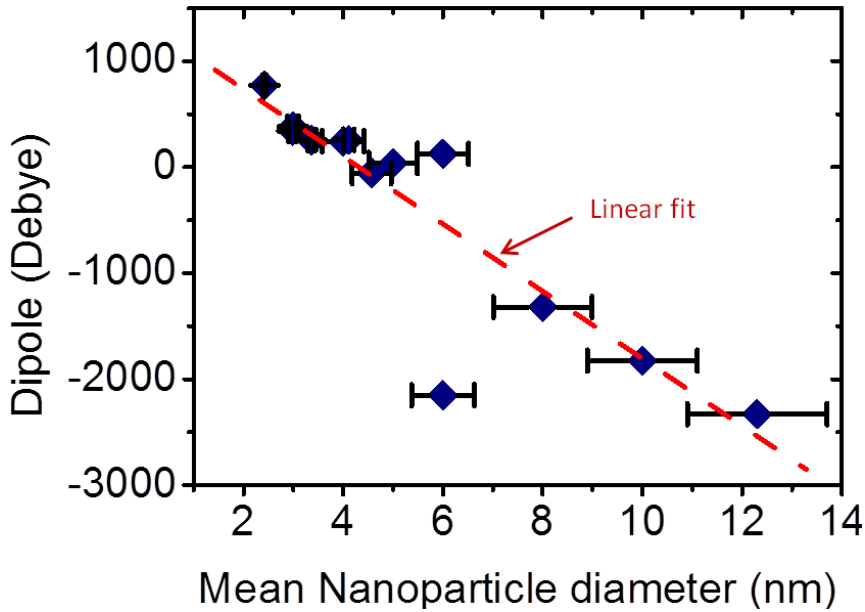


Fig. 5. Calculated dipole reduced with increasing particle diameter, being negative for particles > 6 nm.

The subsequent decrease in dipole and negative values measured for large nanoparticles ≥ 6 nm is due to depolarization effects, notably: (i) increase in atomic columns with particle size causes the electron wave functions in the bulk-like particle to overlap and (ii) increased disordered grain boundaries results in a changing normal vector to the gold surface at each point. This leads to several induced dipole moments with different signs along the grain boundaries, (Wang *et al.*, 2006). Additionally, these grains may also act as electron traps for generated charge. These factors have a net effect of lowering the net dipole. Such similar dipole effects can be obtained by application of metals with different work functions (Uchoa *et al.*, 2008; Huard *et al.*, 2008; Gong *et al.*, 2010). However, besides requiring careful control of the morphologies, the different metals cannot be applied at a single interface.

5.0 Conclusion

A high dependence in electron dipole is demonstrated for graphite surface contacted with Au nanoparticles of varying sizes and coverage. A large value is measured for small nanoparticles. This behaviour is described by charge densities created from individual nanoparticles with small ones having high surface atom densities. The subsequent decrease in dipole with particle diameter is attributed to effects of polarization. The study provides a novel way to produce varying electronic structures at metal-graphite interface so that better devices and applications can be developed.

References

- Barnard A and Chen Y (2011). Kinetic modelling of the shape-dependent evolution of faceted gold nanoparticles. *Journal of Materials Chemistry*, 21, 12239-12245.
- Benayad A, Shin H, Park H Yoon S, Kim K, Jin M, Jeong H, Lee J, Choi J and Lee Y (2009). Controlling work function of reduced graphite oxide with Au-ion concentration. *Chemical Physics Letters*, 475((1-3)), 91-95.
- Blanter Y and Martin I (2007). Transport through normal metalgraphene contacts. *Physical Review B*, 76(15), 155433.
- Corain B and Toshima N (2008). *Metal Nanoclusters in Catalysis and Materials Science*. Elsevier.
- Datta S, Strachan D, Mele E, and Johnson A (2008). Surface potentials and layer charge distributions in few-layer graphene. *Nano Letters*, 9(1), 7-11.
- Gai P and Harmer M (2002). Surface atomic defect structures and growth of gold nanorods. *Nano Letters*, 2(7), 771-774.
- Gefen Y, Shih W, Laibowitz R and Viggiano (1986). Nonlinear behavior near the percolation metal-insulator transition. *Physical review letters*, 57(24), 3097-3100.
- Giovannetti G, Khomyakov P, Brocks G, Karpan V, van den Brink J and Kelly P (2008). Doping graphene with metal contacts. *Physical review letters*, 101(2), 26803.
- Gong C, Lee G, Shan B, Vogel E, wallace R and Cho K (2010). First-principles study of metalgraphene interfaces. *Journal of Applied Physics*, 108, 123711.
- Hamada I and Otani M (2010). Comparative van der Waals density-functional study of graphene on metal surfaces. *Physical Review B*, 82(15), 153412.
- Hayashi N, Ishii H, Ouchi Y and Seki K (2002). Examination of band bending at buckminsterfullerene (C60)/metal interfaces by the Kelvin probe method. *Journal of Applied Physics*, 97(2), 3784.
- Huard B, Stander N, Sulpizio J and Goldhaber-Gordon D (2008). Evidence of the role of contacts on the observed electron-hole asymmetry in graphene. *Physical Review B*, 78(12), 121402.
- Jacobs H, Knapp H, Muller S and Stemmer A (1997). Surface potential mapping: A qualitative material contrast in SPM. *Ultramicroscopy*, 69(1), 39-49.
- Jin K, Choi S S and Jhi S (2010). Crossover in the adsorption properties of alkali metals on graphene. *Physical Review B*, 82(3), 033414.
- Kelvin G and Lassabatere (1898). *Philosophy Magazine*, 46 (80)
- Kikukawa A, Hosaka S and Imura R (1995). Silicon pn junction imaging and characterizations using sensitivity enhanced Kelvin probe force microscopy. *Applied physics letters*, 66, 3510.
- Klusek Z, Dabrowski P, Kowalcyk P, Kozłowski W, Olejniczak W, Blake P, Szybowicz M and Runka T (2009). Graphene on gold: Electron density of states studies by scanning tunneling spectroscopy. *Applied Physics Letters*, 95(11), 113114-113114.

- Liu H, Liu Y and Zhu D (2011). Chemical doping of graphene. *Journal of Materials Chemistry*, 21(10), 3335.
- Lu Y, Munoz M, Steplecaru C, Hao C, Bai M, Garcia N, Schindler K and Esquinazi P (2006). Electrostatic Force Microscopy on Oriented Graphite Surfaces: Coexistence of Insulating and Conducting Behaviors. *Physical Review Letters*, 97(7), 1-4.
- Marks (1994). Experimental studies of small particle structures. *Reports on Progress in Physics*, 57, 603.
- Netterfield R and Martin P (1986). Nucleation and growth studies of gold films prepared by evaporation and ion-assisted deposition. *Applied surface science*, 25, 265-278.
- Nonnenmacher M, O'Boyle M and Wickramasinghe (1991). Kelvin probe force microscopy. *Applied Physics Letters*, 58(25), 2921.
- Nonnenmacher M, O'Boyle M and Wickramasinghe (1992). Surface investigations with a Kelvin probe force microscope. *Ultramicroscopy*, 42-44, 268-273.
- Norrmann S, A. T. (1978). Optical properties of discontinuous gold. *Physical Review B*, 18(2), 674-695.
- Ohgi T and Fujita D (2003). Single electron charging electron effects in gold nanoclusters on alkanedithiol layers with different molecular lengths. *Surface science*, 532, 294-299.
- Palermo V, Palma M and Samori P (2006). Electronic Characterization of Organic Thin Films by Kelvin Probe Force Microscopy. *Advanced Materials*, 18(2), 145-164.
- Rosenwaks Y, Shikler R, Glatzel T and Sadewasser (2004). Kelvin probe force microscopy of semiconductor surface defects. *Physical Review B*, 70(8), 1-7.
- Rusu P, Giovannetti G, Weijtens C, Coehoorn R and Brocks G (2010). First-principles study of the dipole layer formation at metal-organic interfaces. *Physical Review B*, 81(12), 125403.
- Somorjai G (1981). *Introduction to surface chemistry and catalysis*. Canada: Wiley.
- Sun Z, Lu J and Song X (2010). Observation of silicon surfaces using ultrahigh vacuum nc-AFM. *Vacuum*, 85(2), 297-301.
- Sutter P, Flege J and Sutter E (2008). Epitaxial graphene on ruthenium. *Nature materials*, 7(5), 406-411.
- Tang W (2003). Surface roughness and resistivity of Au substrate. *Microelectronic Engineering*, 66(1-4), 445-450.
- Uchoa B, Lin C and Neto A (2008). Tailoring graphene with metals on top. *Physical Review B*, 77(3), 035420.
- Veith G, Lupini A, Rashkeev S, Pennycook S, Mullins D, Schwartz V, Bridges C and Dudney N (2009). Thermal stability and catalytic activity of gold nanoparticles supported on silica. *Journal of Catalysis*, 262(1), 92-101.
- Wang J, Yang M, Jellinek J and Wang G (2006). Dipole polarizabilities of medium-sized gold clusters. *Physical Review A*, 74, 023202.

- Young N, Li Z, Chen Y, Palomba S, Di Vece M and Palmer R (2008). Weighing supported nanoparticles: Size-selected clusters as mass standards in nanometrology. *Physical review letters*, 101(24), 246103.
- Zerweck U, Loppacher C, Otto T, Grafstrom S and Eng L (2005). Accuracy and resolution limits of Kelvin probe force microscopy. *Physical Review B*, 71(12), 1-9.